https://doi.org/10.2352/EI.2024.36.7.ISS-283

Intracell Capacitances in Pixel-Level Hybrid Bond Image Sensor Cells

V. Axelrad; SEQUOIA Design Systems, Inc., O. Milic; formerly OMNIVISION

Abstract

Accurate coupling capacitances are a key part in the design of modern image sensor cells [1] due to their high speed requirements, large number of active devices and interconnects, and complex inter-layer dielectric structure. Automation of 3D structure creation integrated with the design flow as well as speed and robustness of capacitance calculation are crucial for a seamless design and optimization flow. Periodicity of image sensor arrays necessitates availability of periodic boundary conditions. High structural complexity (many layout elements, many metal interconnect levels and many dielectric layers) demands efficient numerics for reasonable runtimes.

We apply a new integrated software package CellCap3D [3] to the calculation of image sensor cell capacitances with the specific example application of comparing a Pixel-Level Hybrid Bonding (PLHB) cell to its conventional counterpart where hybrid bonds are only utilized along the periphery of the die. PLHB [2] is a recently proposed approach which introduces an electrical contact between light-sensing (bottom) die and upper die for every pixel. A hybrid-bond, in essence a small-pitch, small-size Cu-Cu contact, now allows addition of extra MOS devices and capacitors to the individual pixel, thus greatly expanding imager functionality and performance. Additional benefit is achieved in simplification of the manufacturing of the light-sensing die. A reduction in the number of manufacturing steps, also reduces the chance of defect introduction.

The architecture of the simulation system [3], some key components and numerical aspects are discussed in this work. The software produces a complete capacitance matrix for a typical image sensor cell with 5-7 interconnect layers in minutes on a standard Linux machine. Lithographic distortions of layout patterns, as demonstrated in the example in this work, can be optionally included for more physically accurate capacitances. Misalignment of mask layers or bonded wafers relative to each other can be considered for its effects on coupling capacitances. Periodic boundary conditions can be used for periodically repeated image sensor cells, avoiding the need to simulate an array of cells to provide the correct electrostatic environment for one cell.

Introduction: Image Sensor Arrays

Image sensors are a key semiconductor product used in billions of consumer, industrial, automotive and other applications [1]. An image sensor typically contains an array of identical cells, each with a photosensitive device, a number of MOSFETs and several layers of interconnect. Coupling capacitances (intra-cell) between electrical nodes of each cell as well as cell-to-cell capacitances (inter-cell) are needed for design and optimization of image sensors.

A typical 4-transistor (4T) image sensor cell schematic is shown in Fig. 1. In this study we use a common variation of this cell with 4 separate photodiodes (PD) and one shared Floating Diffusion (FD). Each photodiode is one pixel, so in this configuration 4 pixels share one FD and control circuit.

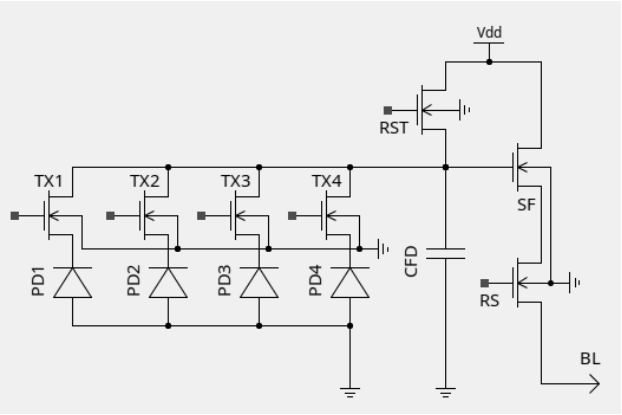

Figure 1. *4-transistor image cell schematic. The cell used in this work is a common configuration with 4 separate pixel photodiodes PD1/2/3/4 sharing one Floating Diffusion FD. The 4 transfer gates TX1/2/3/4 are arranged around the floating diffusion in a diamond pattern as seen in the layouts in Fig. 2.*

FD is the capacitor where conversion from charge (stored electrons) to voltage happens (V=Q/C). Generally, we want the capacitance of FD to be large enough so that all electrons from PD can be transferred to it and converted to a voltage. The reverse-biased photodiode is essentially a capacitor with its own capacitance value, frequently expressed in the maximum number of electrons it is capable of storing before saturating. Therefore, the full-well-capacity of the PD (FWC in number of electrons n_e) when transferred to FD should not saturate the FD due to too low capacitance. The dynamic range is determined by the equation $20 \cdot log_{10} \times n_e/s$ divided by noise in (e/s). Assuming noise is 1e/s, this comes to $20 \cdot log_{10} \times FWC$. If the dynamic range is limited by the FD capacitance, then adding an additional capacitor in parallel can help. In addition to that a variable conversion gain functionality can be easily implemented in pixels due to availability of multitude of capacitor structures like metal-to-metal or MiM.

Stray capacitances add to the noise, specifically fixed-pattern-noise, where signal traces couple to FD and modify its potential due to capacitive coupling. This type of coupling needs to be minimized as much as possible, by moving offending metal traces or by shielding them.

Moving a majority of signal metal traces to the upper wafer minimizes the fixed-pattern noise as distance to FD metal is larger. Improvements to power and speed are not significant, as PLHB

does not reduce the capacitive loading on signaling traces significantly.

PLHB vs. Conventional Cells

PLHB [2] is a novel type of image sensor cells, characterized by pixel-level bonded cells with photosensitive devices and control circuits manufactured on separate wafers. Our PLHB cell layout, cross-section, 3D cell and a conventional cell layout for comparison are shown in Fig. 2. Both cells are standard 4T designs with 4 transfer gates around the floating diffusion arranged in a diamond pattern. PLHB keeps the FD in the bottom wafer separate from the wiring and control transistors in the top wafer (Fig. 2). The PLHB cell layout is visibly simpler and avoids curved metal wires. Litho distortions are included in both cell models by considering corner rounding of the Cnt,Via,M1 layers.

A 3D structural model of the image sensor cell is created in order to calculate internal coupling capacitances. This model shown in Fig. 2 is obtained by polygon extrusion from a) layout supplied as a gds file and b) layer information such as thicknesses and vertical coordinates for metals, as well as dielectric constants for all dielectrics. Electrically connected nets within the cell are traced by assembling conductive pieces in physical contact within layers as well as layer-to-layer. Names are assigned to these nets either via gds text labels or from the simulation control script.

Numerics and Performance

The cell 3D model is next discretized on an automatically generated tensor-product mesh (Fig. 3). To calculate each column j of the capacitance matrix (capmat) for the cell, a non-zero potential V_j is applied to net_j responsible for column j with all other $nets$ at 0. The potential distribution u_j is then calculated by solving the Laplace equation eq. 1. From the electric potential u_j (e.g. Figs. 3, 8) and with electric displacement eq. 2 we calculate the charge Q_i on each net_i as a Gaussian integral eq. 3 over its surface and finally obtain the coupling capacitance $C_{i,j}$ eq. 4.

$$\nabla\varepsilon\nabla u = 0, \quad with \;\; u(net_j) = V_j \tag{1}$$

$$\vec{D} = -\varepsilon\nabla u \tag{2}$$

$$Q_i = \oiint_{Surface(net_i)} \vec{D}\cdot d\vec{n} \tag{3}$$

$$C_{i,j} = dQ_i/dV_j \tag{4}$$

The Laplace solver is iterative and fully parallelized for fast performance on modern multi-core processors, with a complete capmat calculated in a few minutes for a typical image sensor cell. Convergence behavior of the iterative linear solver for the PLHB cell discussed here is shown in Fig. 4. The convergence rate for each electrical net is determined by its physical environment.

Capacitance Matrix

Capacitance matrices calculated for the conventional and PLHB cells (Fig. 2) are shown in Figs. 5, 6. Both cells have similar layout styles and the same circuit topology. Among differences in capacitance values, the PLHB cell shows $\sim 50\%$ increase in FD node capacitance. As a consequence, PLHB has better dynamic range in addition to improved quality photodiode due to physical separation of bonded top and bottom wafers and simpler layout.

Cell Environment and Boundary Conditions

An image sensor cell is typically repeated periodically for millions of pixels in an image sensor array. Periodic boundary conditions (PBC) are therefore a natural choice for accurate capacitance simulations at minimal computational cost. However, some simulation tools only offer homogeneous Neumann or reflective boundary conditions (RBC). For a single-cell simulation we expect that PBC vs RBC would make some noticeable difference in capacitances, larger differences for nets closer to cell boundaries and smaller for nets well separated from such boundaries.

Single Cell with PBC vs RBC

As a simulation experiment, we compare the capacitance matrix for the PLHB cell obtained with PBC and RBC in Fig. 6. Differences in self- and coupling capacitances vary depending on how close the net is to the simulation boundary. For the critical FD (floating diffusion) net we see a 17% difference between PBC and RBC, for GND0 net the difference is 52% due to its proximity to cell boundary. Some nets are far away from cell boundaries and PBC vs RBC results are much closer (RS, TX2/3/4).

3x3 Array to Mimic Periodicity

A common technique to model periodic cells with tools not offering PBC is to surround a center cell with copies of itself to create a periodic environment. For the PLHB cell we can thus construct a 3x3 array shown in Fig. 7. The purpose of the surrounding 8 cells is to mimic periodicity for the center cell. In this case the capacitance matrix of the center cell becomes insensitive to the boundary conditions as shown by small differences for PBC vs RBC capmats in Fig. 7.

Truncated 3x3 Array

A variation of the 3x3 array technique is the truncated 3x3 array, where the 8 outside cell copies are cut off at cell centers Fig. 8. This approach provides a similar level of insensitivity to boundary conditions at reduced calculation runtime by approximately $4/9$ – the ratio of array areas (the actual runtime ratio depends on the linear solver and settings). Both 3x3 array techniques can be replaced by a single cell 1x1 simulation with periodic boundary conditions with very similar capacitance values at much lower computational cost.

When comparing capacitance values in Figs. 6, 7, 8 keep in mind that depending on net connectivity across neighboring cells some net areas and their capacitances in the larger arrays increase by a factor 3 (row or column connections) or 9 (row and column connections, as is the case for ground nets) for the 3x3 array and 2 or 4 for the truncated 3x3 array in comparison to single cell capacitances. Other nets, such as FD, are local to each cell and their capacitances can be compared directly among Figs. 6, 7, 8.

Comparison to Current State-of-the-Art

Full-chip capacitance extractors rely on approximative calculation methods for performance reasons, so they can handle large structures. A numerical PDE (Partial Differential Equation) solver does not rely on any fitting parameters but instead solely on the geometric accuracy of the submitted structure and physical constants. CellCap3D uses a numerical PDE solver and is as accurate as its input, that is the simulation structure given to it, in-

cluding the layout, metal and dielectric layer thicknesses and their properties, process-related effects such as corner rounding, etc.

Some discretization errors are intrinsic to numerical calculation due to finite mesh size but are in general small, typically $< 1-2\%$. These errors can be estimated and controlled by the usual numerical methods such as re-running the calculation with a finer mesh to determine sufficient mesh density. Discretization errors in a numerical solver can be in general traded for simulation time.

Current state of the art numerical interconnect tools offer poor integration into the flow (lack direct gds file import) and do not offer periodic boundary conditions (PBC). External tools are typically used to create the 3D interconnect structure for simulation, adding an engineering and CPU burden. Simulation of periodic designs without PBC requires modeling a small 2x2 or 3x3 array to mimic periodicity with available reflective boundary conditions (RBC), again adding to the engineering and CPU burden.

Our new tool CellCap3D addresses both issues, it is fully integrated into the design flow with direct import from gds files for superior efficiency and ease-of-use. Periodic boundary conditions are natural for periodic arrays such as image sensors, therefore their use reduces the setup and analysis effort, as well as CPU time.

Conclusions

A comparison of coupling intra-cell capacitances in PLHB and conventional image sensor cells is presented. PLHB keeps the FD in the bottom wafer separate from the wiring and control transistors in the top wafer. FD node capacitance is increased and overall layout quality is improved in the PLHB cell.

An integrated and efficient tool for the rapid calculation of within-cell and cell-cell coupling capacitances for image sensors is described. The tool implements periodic boundary conditions and directly imports gds layouts for physical accuracy, efficiency and ease-of-use with minimal user involvement. Efficient numerics and parallelization allow the calculation of a complete cell capacitance matrix in minutes (in many cases seconds) on a desktop machine.

A study of different approaches to model cell periodicity is also shown, comparing single cell simulation with periodic versus reflective boundary conditions, as well as embedding the cell under consideration in a larger 3x3 array or truncated 3x3 array to create a quasi-periodic environment. Such embedding approaches are typically used when periodic boundary conditions are not available in the solver. Single cell simulation with periodic BC is demonstrated to produce results equivalent to those obtained with a 3x3 array at much lower computational cost (by $\simeq 9$x).

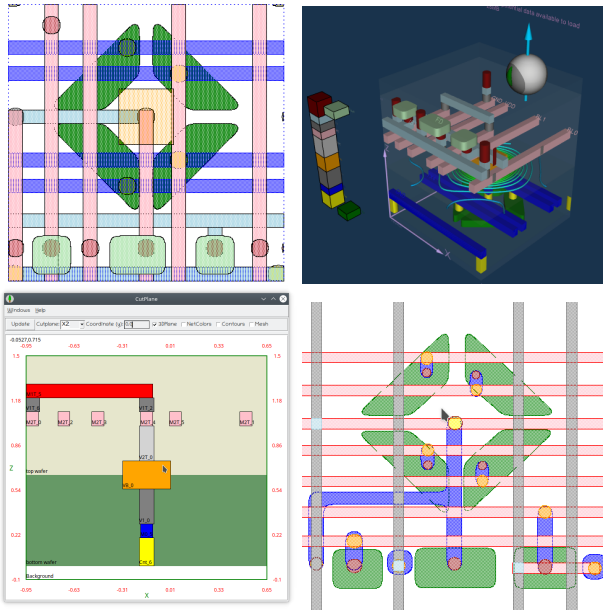

Figure 2. *Pixel-Level Hybrid Bond cell: PLHB layout, 3D model with potential contours in a horizontal XY cutplane through the bonding pad, XZ cross-section, conventional cell layout for comparison. In the cross-section the bottom wafer oxide is shown in dark green, top wafer oxide in light yellow, the bonding pad in orange, etc. Process-induced corner rounding is considered in poly and contact layer patterns.*

References

[1] https://semiengineering.com/cmos-image-sensors-cis-past-present-future/

[2] Vincent C. Venezia, Alan Chih-Wei Hsiung, Kelvin Ai, Xiang Zhao, Zhiqiang Lin, Duli Mao, Armin Yazdani, Eric A. G. Webster, and Lindsay A. Grant, "1.5µm Dual Conversion Gain, Backside Illuminated Image Sensor Using Stacked Pixel Level Connections with 13ke^- Full-Well Capacitance and 0.8e^- Noise," IEDM 2018

[3] SEQUOIA CellCap3D Software, Sequoia Design Systems, 2022-2023.

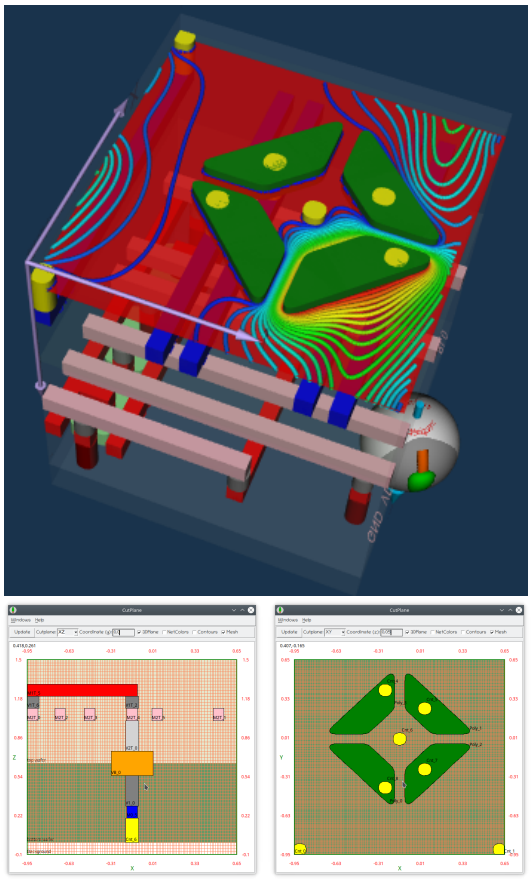

Figure 3. *Electric potential contours in the XY (horizontal) cutplane through the transfer gates, periodic boundary conditions are visible. Automatically generated discretization mesh in the vertical XZ and XY planes.*

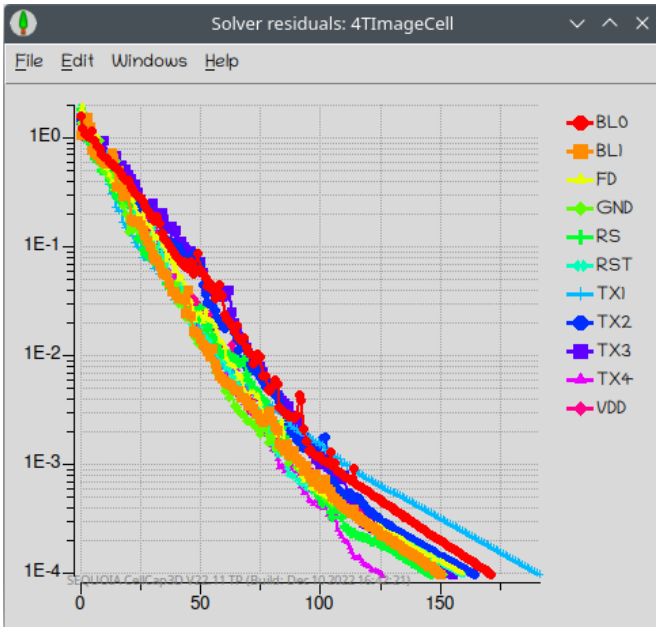

Figure 4. *Convergence behavior of the linear solver for each net depends on the net's physical environment.*

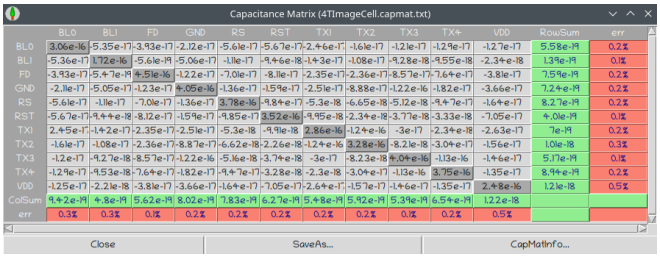

Figure 5. *Cell capacitance matrix for the conventional cell. In comparison, the floating diffusion node FD has $\simeq 50\%$ larger capacitance in the PLHB case (see Fig. 6), helping improve the dynamic range of the cell. Runtimes for the full matrix are $\simeq 30secs$ on an 8-core machine for PLHB and conventional cases. Including process-induced corner rounding on poly and contact layer as shown in Fig. 2 increases runtime to $\simeq 90secs$.*

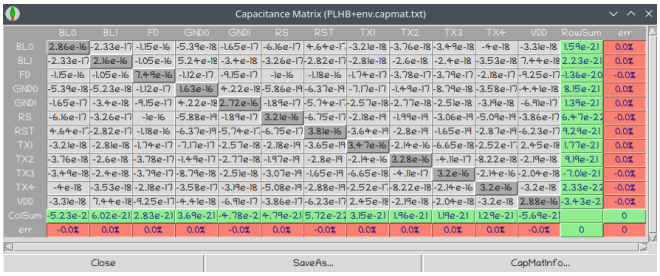

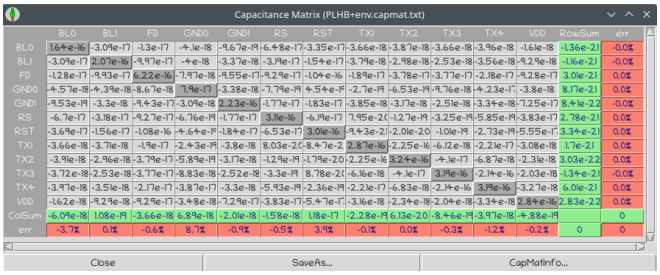

	BL0	BL1	FD	GND0	GND1	RS	RST	TX1	TX2	TX3	TX4	VDD
BL0	**43%**	−33%	89%	24%	94%	−5%	28%	−14%	−3%	−5%	1%	51%
BL1	−33%	**4%**	5%	24%	1%	2%	45%	−35%	−15%	−5%	−1%	−25%
FD	89%	5%	**17%**	29%	−4%	7%	12%	−9%	0%	1%	0%	0%
GND0	15%	16%	23%	**52%**	20%	−33%	29%	100%	96%	−11%	−18%	14%
GND1	94%	3%	−3%	27%	**18%**	6%	68%	−50%	−14%	0%	−5%	−5%
RS	−9%	2%	7%	−15%	6%	**3%**	8%	64%	36%	−6%	−15%	1%
RST	20%	45%	8%	27%	68%	3%	**21%**	97%	93%	39%	5%	11%
TX1	−14%	−32%	−9%	100%	−48%	63%	98%	**17%**	−5%	8%	12%	−26%
TX2	−4%	−14%	0%	96%	−14%	35%	94%	−5%	**1%**	0%	16%	−5%
TX3	−7%	−5%	1%	0%	0%	−7%	47%	7%	0%	**0%**	0%	0%
TX4	1%	1%	0%	−8%	−3%	−17%	18%	12%	17%	0%	**0%**	−2%
VDD	51%	−25%	0%	21%	−5%	1%	12%	−29%	−7%	0%	−4%	**1%**

Figure 6. *PLHB single cell capacitance matrices obtained with periodic boundary conditions (PBC, top), reflective BC (RBC, center image). Differences between PBC and RBC are shown in the bottom image, for diagonal entries of the capmat (self-capacitances) up to 52%. The important FD (floating diffusion) net shows a moderate but significant 17% difference.*

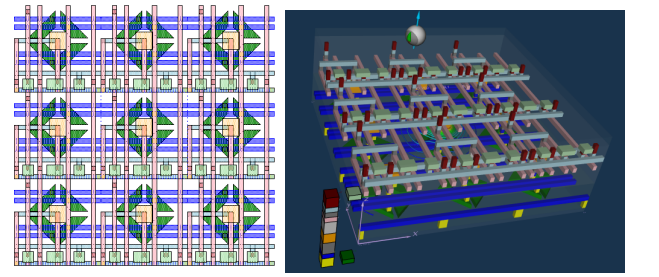

Capacitance Matrix (PLHB+env.capmat.txt)

	BL0	BL1	FD	GND0	GND1	RS	RST	TX1	TX2	TX3	TX+	VDD
BL0	8.67e-16	-7.26e-17	-9.44e-18	5.42e-18	-8.7e-19	-6.61e-17	-4.76e-17	-3.59e-18	-4.1e-18	-3.79e-18	-4.35e-18	-2.55e-18
BL1	-7.26e-17	6.38e-16	-9.75e-17	-4.81e-18	-4.9e-18	-3.23e-17	-2.63e-17	-2.91e-18	-2.6e-18	-2.39e-18	-3.51e-18	-2.21e-17
FD	-9.44e-18	-9.75e-17	7.31e-16	-6.56e-18	-9.05e-17	-9.83e-17	-1e-16	-1.61e-17	-3.64e-17	-3.7e-17	-2.15e-17	-8.69e-17
GND0	5.42e-18	-4.81e-18	-6.56e-18	4.95e-16	-4.03e-18	-1.5e-18	-1.6e-18	-7.33e-19	-1.86e-18	-2.9e-17	-1.07e-16	-4.15e-18
GND1	-8.72e-19	-4.9e-18	-9.05e-17	-4.04e-18	8.35e-16	-1.95e-17	-5.62e-17	-2.74e-18	-2.88e-18	-2.58e-18	-3.3e-18	-2.19e-16
RS	-6.61e-17	-3.23e-17	-9.83e-17	-1.5e-18	-1.95e-17	9.85e-16	-1.97e-16	-1.18e-19	-2.76e-19	-8.13e-19	-1.43e-18	-4.08e-17
RST	-4.76e-17	-2.63e-17	-1e-16	-1.6e-18	-5.62e-17	-1.97e-16	1.09e-15	-1.61e-20	-4.56e-20	-2.54e-19	-6.88e-19	-5.83e-17
TX1	-3.59e-18	-2.91e-18	-1.61e-17	-7.29e-19	-2.74e-18	-1.18e-19	-1.62e-20	1.09e-15	-6.77e-16	-1.88e-17	-7.35e-17	-2.58e-18
TX2	-4.1e-18	-2.6e-18	-3.64e-17	-1.86e-18	-2.88e-18	-2.76e-19	-4.6e-20	-6.77e-16	1.04e-15	-1.26e-16	-2.35e-17	-2.23e-18
TX3	-3.79e-18	-2.39e-18	-3.7e-17	-2.9e-17	-2.58e-18	-8.12e-19	-2.54e-19	-1.88e-17	-1.26e-16	1.01e-15	-6.77e-16	-2.06e-18
TX+	-4.35e-18	-3.51e-18	-2.15e-17	-1.07e-16	-3.3e-18	-1.43e-18	-6.88e-19	-7.35e-17	-2.35e-17	-6.77e-16	1.01e-15	-3.26e-18
VDD	-2.55e-18	-2.21e-17	-8.69e-17	-4.15e-18	-2.19e-16	-4.08e-17	-5.83e-17	-2.57e-18	-2.23e-18	-2.06e-18	-3.26e-18	8.58e-16
Z+	-3.6e-18	-2.91e-18	-2.05e-18	-2.11e-16	-2.75e-18	-5.41e-19	-1.05e-18	-1.06e-19	-2.77e-19	-4.08e-18	-1.35e-17	-2.58e-18
Z5	-4.1e-18	-2.6e-18	-9.96e-19	-5.15e-17	-2.88e-18	-2.96e-19	-7.51e-19	3.48e-20	-1.1e-19	-2.27e-18	-5.35e-18	-2.23e-18

Close SaveAs... CapMatInfo...

Capacitance Matrix (PLHB+env.capmat.txt)

	BL0	BL1	FD	GND0	GND1	RS	RST	TX1	TX2	TX3	TX+	VDD
BL0	8.6e-16	-7.52e-17	-9.44e-18	5.42e-18	-1.18e-18	-6.61e-17	-4.76e-17	-3.59e-18	-4.1e-18	-3.79e-18	-4.35e-18	-2.95e-18
BL1	-7.53e-17	6.3e-16	-9.75e-17	-4.81e-18	-6.23e-18	-3.23e-17	-2.63e-17	-2.91e-18	-2.6e-18	-2.39e-18	-3.51e-18	-2.4e-17
FD	-9.44e-18	-9.75e-17	7.31e-16	-6.56e-18	-9.05e-17	-9.83e-17	-1e-16	-1.61e-17	-3.64e-17	-3.7e-17	-2.15e-17	-8.69e-17
GND0	5.42e-18	-4.81e-18	-6.56e-18	4.96e-16	-4.04e-18	-1.52e-18	-1.61e-18	-7.39e-19	-1.84e-18	-2.9e-17	-1.07e-16	-4.15e-18
GND1	-1.18e-18	-6.17e-18	-9.05e-17	-4.04e-18	8.01e-16	-1.95e-17	-5.62e-17	-2.74e-18	-2.88e-18	-2.58e-18	-3.3e-18	-2.21e-16
RS	-6.61e-17	-3.23e-17	-9.83e-17	-1.51e-18	-1.95e-17	9.85e-16	-1.97e-16	-1.17e-19	-2.8e-19	-8.22e-19	-1.43e-18	-4.08e-17
RST	-4.76e-17	-2.63e-17	-1e-16	-1.61e-18	-5.62e-17	-1.97e-16	1.09e-15	-1.55e-20	-4.51e-20	-2.54e-19	-6.88e-19	-5.83e-17
TX1	-3.59e-18	-2.91e-18	-1.61e-17	-7.25e-19	-2.74e-18	-1.18e-19	-1.54e-20	1.09e-15	-6.76e-16	-1.85e-17	-7.39e-17	-2.58e-18
TX2	-4.1e-18	-2.6e-18	-3.64e-17	-1.83e-18	-2.88e-18	-2.83e-19	-4.56e-20	-6.77e-16	1.04e-15	-1.26e-16	-2.33e-17	-2.23e-18
TX3	-3.79e-18	-2.39e-18	-3.7e-17	-2.89e-17	-2.58e-18	-8.27e-19	-2.56e-19	-1.86e-17	-1.26e-16	1.01e-15	-6.76e-16	-2.06e-18
TX+	-4.35e-18	-3.51e-18	-2.15e-17	-1.07e-16	-3.3e-18	-1.43e-18	-6.9e-19	-7.38e-17	-2.31e-17	-6.76e-16	1.01e-15	-3.26e-18
VDD	-2.96e-18	2.42e-17	-8.69e-17	-4.15e-18	-2.21e-16	-4.08e-17	-5.83e-17	-2.58e-18	-2.23e-18	-2.06e-18	-3.26e-18	8.55e-16
Z+	-3.6e-18	-2.91e-18	-2.05e-18	-2.1e-16	-2.75e-18	5.44e-19	-1.05e-18	-1.08e-19	-2.75e-19	-4.09e-18	-1.35e-17	-2.58e-18
Z5	-4.09e-18	-2.59e-18	-9.97e-19	-5.13e-17	-2.87e-18	-3.03e-19	-7.57e-19	3.27e-20	-1.1e-19	-2.29e-18	-5.35e-18	-2.23e-18

Close SaveAs... CapMatInfo...

rel_diff	BL0	BL1	FD	GND0	GND1	RS	RST	TX1	TX2	TX3	TX4	VDD
BL0	0.8%	0.3%	0.0%	0.0%	0.0%	0.0%	0.0%	0.0%	0.0%	0.0%	0.0%	0.0%
BL1	0.4%	1.3%	0.0%	0.0%	0.2%	0.0%	0.0%	0.0%	0.0%	0.0%	0.0%	0.3%
FD	0.0%	0.0%	0.0%	0.0%	0.0%	0.0%	0.0%	0.0%	0.0%	0.0%	0.0%	0.0%
GND0	0.0%	0.0%	0.0%	−0.2%	0.0%	0.0%	0.0%	0.0%	0.0%	0.0%	0.0%	0.0%
GND1	0.0%	0.2%	0.0%	0.0%	4.1%	0.0%	0.0%	0.0%	0.0%	0.0%	0.0%	0.2%
RS	0.0%	0.0%	0.0%	0.0%	0.0%	0.0%	0.0%	0.0%	0.0%	0.0%	0.0%	0.0%
RST	0.0%	0.0%	0.0%	0.0%	0.0%	0.0%	0.0%	0.0%	0.0%	0.0%	0.0%	0.0%
TX1	0.0%	0.0%	0.0%	0.0%	0.0%	0.0%	0.0%	0.0%	0.0%	−0.1%	0.0%	0.0%
TX2	0.0%	0.0%	0.0%	0.0%	0.0%	0.0%	0.0%	0.0%	0.0%	0.0%	0.0%	0.0%
TX3	0.0%	0.0%	0.0%	0.0%	0.0%	0.0%	0.0%	0.0%	0.0%	0.0%	−0.1%	0.0%
TX4	0.0%	0.0%	0.0%	0.0%	0.0%	0.0%	0.0%	0.0%	0.0%	−0.1%	0.0%	0.0%
VDD	0.0%	0.2%	0.0%	0.0%	0.2%	0.0%	0.0%	0.0%	0.0%	0.0%	0.0%	0.3%

Figure 7. *3x3 cell array constructed by replicating the PLHB cell (layout, 3D cell view - top row, capmat with PBC - 2nd row, capmat with RBC - 3rd row, differences between PBC and RBC relative to diagonal values - bottom row). The capmat of the center cell of the 3x3 array is insensitive to boundary conditions, PBC vs RBC makes little difference. Runtimes for center cell capacitances are* $\simeq 1.5mins$.

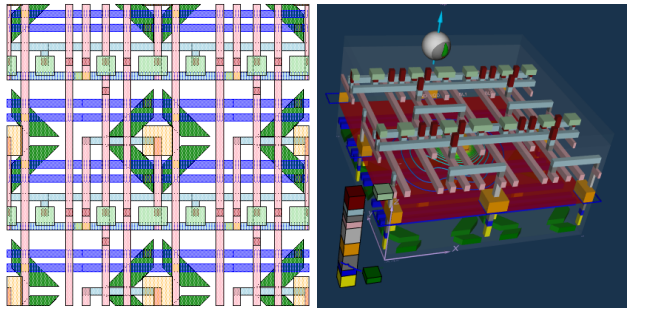

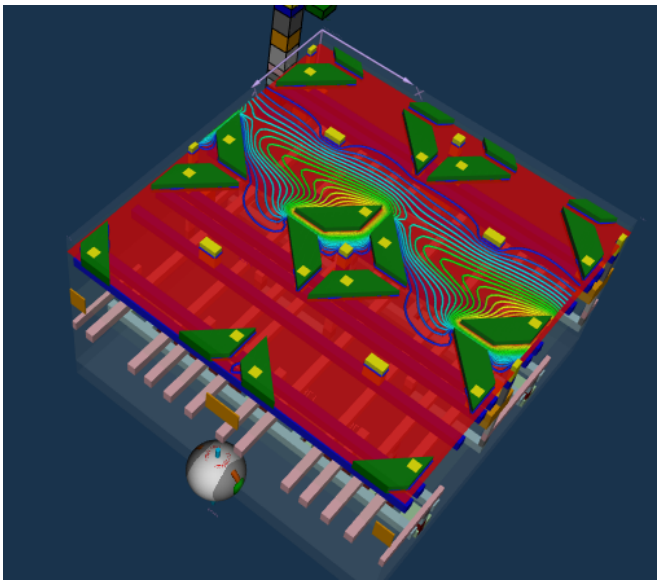

Capacitance Matrix (PLHB+env.capmat.txt)

	BL0	BL1	FD	GND0	GND1	RS	RST	TX1	TX2	TX3	TX+	VDD
BL0	5.8e-16	-4.76e-17	-1.01e-17	5.44e-18	-5.82e-19	-6.63e-17	-4.79e-17	-3.6e-18	-4.08e-18	-3.77e-18	-4.35e-18	-1.79e-18
BL1	-4.76e-17	4.01e-16	-9.04e-17	-4.56e-18	-2.98e-18	-3.07e-17	-2.44e-17	-2.73e-18	-2.38e-18	-2.19e-18	-3.3e-18	-1.41e-17
FD	-1.01e-17	-9.04e-17	7.3e-16	-6.73e-18	-8.86e-17	-9.95e-17	-1.01e-16	-1.64e-17	-3.71e-17	-3.77e-17	-2.19e-17	-8.9e-17
GND0	5.44e-18	-4.56e-18	-6.73e-18	3.31e-16	-3.85e-18	-1.01e-18	-1.09e-18	-5e-19	-1.24e-18	-1.91e-17	-7.17e-17	-4.32e-18
GND1	-5.82e-19	-2.98e-18	-8.86e-17	-3.85e-18	5.44e-16	-1.85e-17	-5.38e-17	-2.62e-18	-2.75e-18	-2.45e-18	-3.13e-18	-1.46e-16
RS	-6.63e-17	-3.07e-17	-9.95e-17	-1.01e-18	-1.85e-17	6.56e-16	-1.29e-16	-7.96e-20	-1.83e-19	-5.4e-19	-9.58e-19	-4.25e-17
RST	-4.79e-17	-2.49e-17	-1.01e-16	-1.09e-18	-5.38e-17	-1.29e-16	7.23e-16	-1.42e-20	-3.17e-20	-1.7e-19	-4.66e-19	-5.95e-17
TX1	-3.6e-18	-2.73e-18	-1.64e-17	-4.98e-19	-2.62e-18	8.04e-20	-1.47e-20	7.27e-16	-4.49e-16	-1.25e-17	-4.9e-17	-2.69e-18
TX2	-4.08e-18	-2.38e-18	-3.71e-17	-1.25e-18	-2.75e-18	-1.83e-19	3.26e-20	-4.49e-16	6.92e-16	-8.36e-17	-1.56e-17	-2.34e-18
TX3	-3.77e-18	-2.19e-18	-3.77e-17	-1.91e-17	-2.46e-18	-5.4e-19	-1.69e-19	-1.25e-17	-8.36e-17	6.72e-16	-4.49e-16	-2.16e-18
TX+	-4.35e-18	-3.3e-18	-2.19e-17	-7.17e-17	-3.13e-18	-9.59e-19	-4.66e-19	-4.9e-17	-1.56e-17	-4.49e-16	6.75e-16	-3.4e-18
VDD	-1.79e-18	-1.41e-17	-8.9e-17	-4.32e-18	-1.46e-16	4.25e-17	-5.95e-17	-2.69e-18	-2.34e-18	-2.16e-18	-3.4e-18	5.83e-16

Close SaveAs... CapMatInfo...

Figure 8. *A common variation of the 3x3 array approach truncates the 8 surrounding cells at their centers to save runtime with only little penalty in accuracy. The center mage shows the potential contours for TX4 at high viewed from the backside, the TX4 connection between all three cells of middle row is visible. The capmat of the center cell is again insensitive to boundary conditions.*